Energy-Efficient Wireless Communications: From Energy Modeling to Performance Evaluation

Farhad Mahmood, *Member, IEEE*, Erik Perrins, *Senior Member, IEEE*, and Lingjia Liu, *Senior Member, IEEE*

***Abstract*—In this paper, we analyze energy-efficient communications based on an advanced energy consumption model for wireless devices. The developed model captures relationships between transmission power, transceiver distance, modulation order, channel fading, power amplifier (PA) effects, as well as other circuit components in the radio frequency transceiver. Based the developed model, we are able to identify the optimal modulation order in terms of energy-efficiency under different situations (e.g., different transceiver distance, different PA classes and efficiencies, different pulse shape, etc). This provides an important framework for analyzing energy-efficient communications for different wireless systems ranging from cellular networks to wireless Internet of Things.**

***Index Terms*—Energy consumption, RF transceiver, multilevel quadrature amplitude modulation (MQAM), power amplifier, Class AB, peak to average ratio, maximum drain efficiency, decay rate, roll-off factor.**

I. Introduction

ENERGY and power consumption are limiting factors in wireless communication systems. Many studies have been conducted in the literature on energy efficiency for new high-data-rate wireless communication systems, such as 5G [1]–[11]. Reducing the energy consumption for wireless systems, in particular base stations, is an important step to reduce the operating cost and greenhouse gas emissions of wireless infrastructure [12]. On top of that, reducing the energy consumption of wireless handsets can extend mobile battery life and mitigate a power amplifier (PA) packaging issue known as the power dissipation capacity [13]. For these reasons and more, the energy consumption of wireless handsets has received increasing attention in recent years [14]–[26].

Detailed discussions of the energy efficiency of wireless communications have been presented in [16] and [17]. However, these models focus mostly on wireless sensor networks for short distances, where throughput is not as big an issue as in wireless cellular systems. Furthermore, the channel that is considered in the model is a basic additive white Gaussian noise (AWGN) (no small scale fading is considered); and the impact of peak-to-average ratio (PAR) on the PA via modulation pulse roll-off factor has been neglected. The effects of PAR on the wireless handset transceiver and RF components are studied in [18], [19]; however, this investigation considers a distance of 10 m between the transmitter and receiver and neglects the impact of the modulation order, b, which is the number of bits per symbol, on the energy. Modulation order is considered in [21], [27]; however, their model is simplistic in other ways and does not consider PAR, transmission distance, or any RF components such as the class of PA.

The issue of which PA to use is an important consideration in its own right. PAs can be categorized as linear or non-linear. Linear PAs such as class A, class AB, and class B have a considerable operating range where they provide the linear amplification required by linear modulations; non-linear PAs such as class E and class F have no linear operating region and are thus more suitable for constant envelope modulations [28]. Linear PAs have lower maximum efficiency than non-linear PAs; however, because linear modulations can provide higher spectral efficiency, we consider linear PAs in this paper. Different classes of linear PAs have different linearity ranges and different levels of efficiency. It is important to know and to model such parameters correctly for each of the PA classes in order to maximize energy efficiency in wireless transceivers.

The objective and contribution of this work is to develop an advanced model for wireless systems to characterize the impact of various communication parameters (e.g., the modulation order, the roll-off factor of the underlying pulse shape, and the transceiver distance) on the amount of energy consumption of various transceiver components. As such, our goal is to obtain the optimal modulation order to maximize the energy-efficiency considering the realistic power consumptions of the power amplifiers dissipated and transmit energy. Central to this task is the importance of an accurate PA model, due to the PAs dominance in transceiver energy consumption. We strive for this accuracy in two ways: (1) we treat the impact of transmitted energy and

Manuscript received November 15, 2018; revised February 15, 2019 and May 4, 2019; accepted May 26, 2019. Date of publication June 6, 2019; date of current version August 13, 2019. This paper was presented in part at the IEEE Global Communications Conference, San Diego, CA, USA, Dec. 2015. The work of F. Mahmood was supported by the U.S. National Science Foundation under Grant CCF-1422241 and the Higher Committee of Education in Iraq. The work of E. Perrins was supported by the U.S. National Science Foundation under Grant CCF-1422241. The work of L. Liu was supported in part by the U.S. National Science Foundation (NSF) under Grants ECCS-1802710, ECCS-1811497, and CNS-1811720 and in part by U.S. National Science Foundation under Grant CCF-1422241. The review of this paper was coordinated by Prof. Y. Zhou. *(Corresponding author: Farhad Mahmood.)*

F. Mahmood is with the Department of Electrical Engineering and Computer Science, University of Kansas, Lawrence, KS 66045 USA, and also with the Department of Electrical Engineering, University of Mosul, Mosul 41001, Iraq (e-mail: farhad.m@uomosul.edu.iq).

E. Perrins is with the Department of Electrical Engineering and Computer Science, University of Kansas, Lawrence, KS 66045 USA (e-mail: esp@ieee.org).

L. Liu is with the Bradley Department of Electrical and Computer Engineering, Virginia Tech, Blacksburg, VA 24060 USA (e-mail: ljliu@vt.edu).

Digital Object Identifier 10.1109/TVT.2019.2921304

dissipated energy (heat) separately so the effect of each is clearly understood; and (2) we model multiple classes of PA depending on their characteristics and on their behavior with modulated signals. The simultaneous requirement for spectrum efficiency and energy efficiency has driven the pairing of spectrally-efficient multilevel quadrature amplitude modulation (MQAM) with relatively energy-efficient class AB PAs [29], [30]. However, most energy efficiency models in the literature neglect this fact and are based on class A PAs with a fixed efficiency, cf. e.g. [16]–[20]. In this paper we model different linear PAs with the associated maximum drain efficiency and decay rate—which to the best of our knowledge is a first for wireless handset models to jointly study these parameters—in order to provide practical design insights. Further, using our model, it will be easier to observe the impact of different parameters such as PAR on the PA and hence on the energy efficiency.

Another key issue is to model the separate components of PAR. Such modeling has often been limited to the signal constellation alone, as in [16], [19], [20]. A neglected-yet-significant component of PAR stems from the modulation pulse, which has a roll-off factor and is typically factored into separate square-root-Nyquist pulses at the transmitter and the receiver, which is called square-root raised cosine (SRRC) (the model in [19] ignores this factorization). Accurate consideration of the roll-off factor is essential for correct modeling of energy consumption and the required bandwidth.

Based on the above motivation, our energy consumption model takes into account parameters such as transmitted energy, dissipated energy, other circuit energies, constellation size, modulation pulse roll-off factor, normalized transmission time (or transmission duty cycle), Rayleigh fading channel, PA's maximum drain efficiency, PA's efficiency decay rate, and transmission distance. We use our model to generate a comprehensive set of numerical results that give design insights such as: Which modulation order/normalized transmission time pairing is most energy efficient for a given transmission distance? How much power back-off is required for the PA to transmit a high modulation order? What is the impact of PA selection on energy consumption as a function of modulation order and normalized transmission time? In our preliminary work on this problem [31], our focus was mainly on modeling the various circuit energies, including the separate modeling of the PA's transmitted and dissipated energies. This paper contributes important practical enhancements, which include the Rayleigh fading, the modeling of PA efficiency with the appropriate drain efficiency and decay rate, factoring the PAR into its several components, and determining the optimum modulation order for energy efficiency at a given distance. These enhancements allow our model to fill important gaps in our understanding left by previous studies, including our own.

The remainder of this paper is organized as follows. We begin in Section II with the system model, after which we study the transmitted energy in Section III. The circuit energy is discussed in detail in two sections: Section IV discusses the PA dissipated energy and Section V discusses the energy of other transceiver circuits. Section VI formulates the final energy metrics. Finally, the main conclusions are summarized in Section VII.

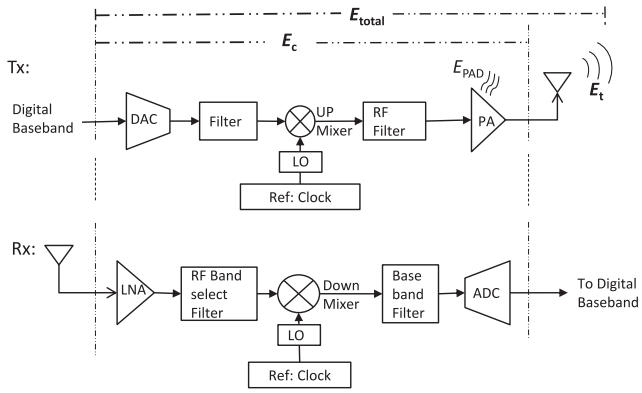

Fig. 1. Block diagram of the transceiver circuit.

II. System Model

In this paper, we consider a transmission range of $d = 10$ to $d = 200$ m to cover short and long distance communications, respectively. We select the target probability of error in the intended receiver as $p_{e_b} = 10^{-3}$. We consider the Rayleigh fading channel, i.e. small scale fading. We consider MQAM signal constellations of size M and constellation order $b = \log_2 M$. We do not consider error control coding and we assume perfect timing and carrier synchronization.

In this section we outline the RF transceiver blocks of our model, the operation modes, and the corresponding energy consumption model.

A. Transceiver Blocks

The RF transceiver's circuit structure typically includes many RF components as shown in Fig. 1, such as the PA, digital-to-analog converter (DAC), analog-to-digital converter (ADC), low-noise-amplifier (LNA), local-oscillator (LO), filters, mixers, etc. These components can be active or inactive depending on the operation mode of the handset.

B. RF Transceiver Operation Modes

The transceiver operates in one of two modes:

1) *On* (active) mode: when all circuits are active and the signal is being transmitted, with a time of T_{on}, a power level of P_{on}, and energy consumed of $E_{\text{on}} = P_{\text{on}} T_{\text{on}}$.
2) *Sleep* (inactive) mode: when there is no signal to be transmitted and all circuits are off, with a time of T_{sleep}, a power level of P_{sleep}, and energy consumed of $E_{\text{sleep}} = P_{\text{sleep}} T_{\text{sleep}}$.

Accordingly, the total energy consumption of the transceiver is the sum of the energies of these two modes:

$$E_{\text{total}} = E_{\text{on}} + E_{\text{sleep}} = P_{\text{on}} T_{\text{on}} + P_{\text{sleep}} T_{\text{sleep}}, \qquad (1)$$

where P_{sleep} is listed in Table I and E_{on} is developed further in this section. The overall cycle duration is $T = T_{\text{on}} + T_{\text{sleep}}$. We

TABLE I
SYSTEM PARAMETERS

Components	Symbol	Assumed value
Modulation order– under study	b	$\in \mathbb{N}$
Roll-off factor	α	0.42
Overall cycle duration	T	100 mSec
Total bits to be transmitted	L	14 Kbit
Symbol rate	R_{s}	100 KHz
Bit error rate	p_{e_b}	10^{-3}
Thermal noise	$\sigma^2 = N_o/2$	-147 dBm/Hz
Receiver noise figure	N_{F}	10 dB
Propagation loss factor	k	2.6
Other fixed power	P_{fixed}	288 mW
Handset sleep mode power	P_{sleep}	50 mW
Link margin	M_l	4dB

define the normalized *on* time as $\epsilon = T_{\mathrm{on}}/T$. The value of ϵ determines the relative time (or duty cycle) required for the circuits to send a fixed number of L information bits. One extreme case is to have $T_{\mathrm{on}} \to T$ i.e. $\epsilon \to 1$; this is where the circuits never go to sleep. Here the lowest modulation order is selected because the transmitter has sufficient time to transmit the L bits. The other extreme case is to have $T_{\mathrm{on}} \to 0$, i.e. $\epsilon \to 0$ and $T_{\mathrm{sleep}} \to T$; this is where the modulation order must approach infinity ($b \to \infty$) in order to transmit the L bits. For the sake of practicality, we constrain the transceiver to be in the *on* mode at least 10% of the time, i.e., $\epsilon \in [0.1, 1]$, because an arbitrarily large modulation order is infeasible.

There are subtle tradeoffs between the transmission duty cycle, modulation order, and overall energy consumption. As such, it is important to establish the relationships between the many parameters in the energy consumption model. The minimum value of T_{on} is a function of b, L, and the symbol rate R_{s}, and is

$$T_{\mathrm{on}} \geq \frac{L}{R_{\mathrm{s}} b}. \tag{2}$$

The inequality stems from the fact that b must assume integer values. Solved for b, this expression becomes

$$b = \left\lceil \frac{L}{R_{\mathrm{s}} T_{\mathrm{on}}} \right\rceil = \left\lceil \frac{L}{R_{\mathrm{s}} T \epsilon} \right\rceil, \tag{3}$$

where $\lceil y \rceil$ denotes the smallest integer greater than or equal to y (commonly referred to as the ceiling operator). R_{s} is related to the bandwidth of the system, B, via the dimensionality theorem for MQAM [28], where for a raised cosine pulse with roll-off factor α, the bandwidth is given by

$$B = (1 + \alpha) R_{\mathrm{s}}. \tag{4}$$

The impact of α on the PAR and energy consumption will be discussed in Section IV-C. The values of T, R_{s}, and L are fixed and are listed in Table I.

C. Modeling the Energy Consumption

In the *on* mode,[1] the energy consumption in the literature [16]–[20] is usually divided into two main parts: (a) the total PA energy consumption, E_{PA}, which includes the transmit energy E_{t} and the impact of PA efficiency δ as:

$$E_{\mathrm{PA}} = E_{\mathrm{t}}/\delta; \tag{5}$$

and (b) the energy consumption of all other transceiver blocks, which are mentioned in Section II-A excluding the PA, and form E_{others}. In our model, as shown in Fig. 1, we rearrange this combination as (a) the transmit energy E_{t}, and (b) the total circuit energy E_c, which includes E_{others} *and* the impact of PA efficiency δ in the form of waste heat dissipated by the PA, E_{PAD}. The steps going from previous models to ours are

$$\begin{aligned} E_{\mathrm{on}} &= E_{\mathrm{PA}} + E_{\mathrm{others}} \\ &= E_{\mathrm{t}}/\delta + E_{\mathrm{others}} \\ &= (E_{\mathrm{t}} + E_{\mathrm{PAD}}) + E_{\mathrm{others}} \\ &= E_{\mathrm{t}} + (E_{\mathrm{PAD}} + E_{\mathrm{others}}) \\ &= E_{\mathrm{t}} + E_{\mathrm{c}}. \end{aligned} \tag{6}$$

It is worth noting that separating PA efficiency, δ, from E_{t} and isolating it entirely in E_{PAD} is a key step in developing our model. Because of this step, it is easier to identify the true impact of parameters such as b and d on the different energy terms inside the transceiver. For example, the modulation order b affects E_{t} via the required probability of bit error p_{e_b}, while it affects E_{PAD} via the amount of PAR. Furthermore, the impact on the dissipated energy due to parameters such as maximum drain efficiency and decay rate for different classes of PAs will be easier to define.

The following three sections of this paper will discuss the energy terms E_{t}, E_{PAD}, and E_{others}, respectively. Generally, the transmitted energy, $E_{\mathrm{t}} = P_{\mathrm{t}} T_{\mathrm{on}}$, depends on many factors such as link distance d, propagation loss factor, system bandwidth B, receiver noise figure N_{F}, required p_{e_b} at the receiver, modulation order b, and T_{on}. The value of E_{PAD} still depends on E_{t} with respect to δ as

$$E_{\mathrm{PAD}} = (1/\delta - 1)\, E_{\mathrm{t}}. \tag{7}$$

For example, if $\delta = 0.25$, the amount of $E_{\mathrm{PAD}} = 3E_{\mathrm{t}}$. E_{others} that is shown in Fig. 1 is nearly fixed for a given communication distance, d; however, there is some variation because the DAC and ADC energy consumption varies with modulation order b [32]. As such, we enhance our model by treating these separately, which yields

$$E_{\mathrm{others}} = (P_{\mathrm{DAC}} + P_{\mathrm{ADC}} + P_{\mathrm{fixed}})\, T_{\mathrm{on}}, \tag{8}$$

where the value for P_{fixed} is listed in Table I.

It is important to mention that we deal with the uplink scheme; therefore, as we determine E_{t}, the transmitter is in the handset and the receiver is in the base station. However, as we deal with

[1] E_{sleep} is no longer investigated, but it is considered in all the total energy results of this paper.

E_c, we calculate the energy consumed in both the transmitter and receiver sides of the handset, in order to determine the total energy consumption per bit.

III. Transmitted Energy E_t

To achieve a specific constraint on the average probability of bit error at the base station receiver, say $p_{eb} = 10^{-3}$, it is necessary to determine the transmit energy, $E_{\rm t}$ required for the handset PA for transmission over Rayleigh fading channel. The exact analytical formula for the probability of error for MQAM in the Rayleigh fading channel is provided in the literature [33], [34]. However, because of the complexity in determining $E_{\rm t}$ as a function of p_{eb}, we do not consider using the exact formula of [33] herein. In this paper, we derive a simple general formula for MQAM (for even and odd b) based on the derivation that is provided in [35, Section 3.1], and [36, Eq. 6.58] for $b = 1$ and $b = 2$, which are binary phase shift keying (BPSK) and quadratic phase shift keying (QPSK), respectively. The derivation is accomplished by taking the average of the probability of error over the Rayleigh fading probability density function.

For coherent detection, the average probability of error for MQAM in the presence of Rayleigh fading is

$$\bar{p}_{eb} = \mathbb{E}_h \left\{ W \cdot \mathrm{Q}\left(\sqrt{Z \cdot |h|^2 \mathrm{SNR}} \right) \right\}, \tag{9}$$

where SNR is the signal to noise ratio at the receiver and $\mathrm{Q}(\cdot)$ is the Gaussian Q-function. For $b \in \text{even}(\mathbb{N})$ we have $Z = \frac{3}{2^b - 1}$ and $W = \frac{4}{b} \cdot (1 - \frac{1}{\sqrt{2^b}})$; and for $b \in \text{odd}(\mathbb{N})$ we have $Z = \frac{6}{2 \cdot 2^b - 1}$ and $W = \frac{4}{b} \cdot (1 - \frac{3}{2 \cdot 2^b})$ [37, Eq. 6.45]. $\mathbb{E}_h\{\cdot\}$ is the expected value with respect to the distribution of the channel gain $|h|^2$. As we show in Appendix A, with a unit Rayleigh fading channel gain, the probability of error for MQAM is:

$$\bar{p}_{eb} = W \cdot \left(\frac{1}{2} \cdot \left(1 - \sqrt{\frac{Z \cdot \mathrm{SNR}}{2 + Z \cdot \mathrm{SNR}}} \right) \right). \tag{10}$$

To find the required SNR at the receiver, we can write:

$$\mathrm{SNR}(b) = \frac{2}{Z} \cdot \left(\frac{W}{4\, \bar{p}_{eb}} - 1 \right) \approx \frac{W}{2Z} \frac{1}{\bar{p}_{eb}}, \tag{11}$$

where the approximation is valid for a very low probability of error, i.e., $\bar{p}_{eb} \leq 10^{-3}$. We see that for a fixed target $\bar{p}_{eb}$, SNR reduces to a function of only b. From the SNR, we can obtain the received power as

$$P_{\rm r}(b) = 2B\sigma^2 N_{\rm F}\, \mathrm{SNR}(b), \tag{12}$$

where $N_{\rm F}$ is the noise figure of the receiver, $\sigma^2 = \frac{N_0}{2}$ is the noise variance, and N_0 is the noise power spectral density. B is the system bandwidth. At distance d, to achieve $P_{\rm r}(b)$ at the base station the transmitted power from our wireless handset must be

$$P_{\rm t}(b, d) = P_{\rm r}(b)\, G(d), \tag{13}$$

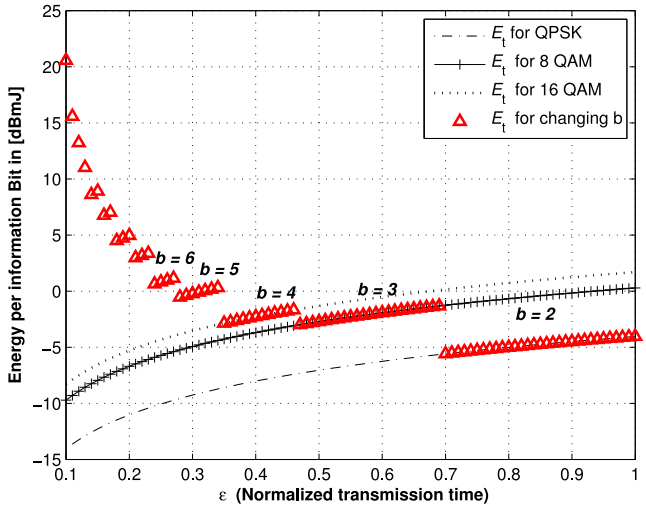

Fig. 2. Comparison of $E_{\rm t}$ with different kinds of QAM for Rayleigh fading at $d = 200$ m.

where $G(d)$ is the distance-based path-loss component[2] (i.e. large scale fading)

$$G(d) = d^k G_1 M_l, \tag{14}$$

where k is the propagation loss factor; M_l is the link margin compensating for the additive background noise or interference; G_1 is the reference path loss attenuation at $d = 1$ m from the transmitter, and is assumed here to be $G_1 = 66$ dB [38]. In practice, k and G_1 vary greatly with the environment, carrier wavelength, base station and handset heights from the ground, and antenna gains. Equation (13) shows the PA transmit power depends on two main parameters b, and d. Thus, $E_{\rm t}$ can be obtained as

$$E_{\rm t}(b, d) \triangleq P_{\rm t}(b, d)\, T_{\rm on} \approx \frac{W}{Z\bar{p}_{eb}} B\sigma^2 N_{\rm F} G(d) T_{\rm on}. \tag{15}$$

Fig. 2 captures the relationship between $E_{\rm t}$ and $T_{\rm on}$ and includes the dependence of b on $T_{\rm on}$ [see (3)]. Fig. 2 shows that to send L bits in a short period of time, say $\epsilon = T_{\rm on}/T = 0.24$, the required value of b, according to (3), is 6 (i.e. 64-QAM) or higher and the required $E_{\rm t}$ is around 1 dBmJ per bit. However, to send the same L bits in a longer period of time, such as $\epsilon = 0.8$, a lower modulation order can be used, such as $b = 2$ (i.e. quadrature phase shift keying modulation, QPSK). This in turn reduces the required $E_{\rm t}$ to around -5 dBmJ per bit, which is much less than that required for $b = 6$. Therefore, increasing ϵ allows the transceiver to use smaller b and hence consume less $E_{\rm t}$. Because b is required to be an integer, as explained in II-B, the $E_{\rm t}$ graph in Fig. 2 takes discrete steps up or down with changing b. Fig. 2 shows reference curves for a few fixed modulations, such as QPSK, 8-QAM, and 16-QAM. Because $E_{\rm t}$ continues to increase slightly with increasing $T_{\rm on}$ but b changes only in discrete steps, the optimum $T^*_{\rm on}$ for each modulation order b is the point where b steps down, which is where (2) is satisfied with equality.

[2]We consider a simple path-loss model for general tradeoff analysis.

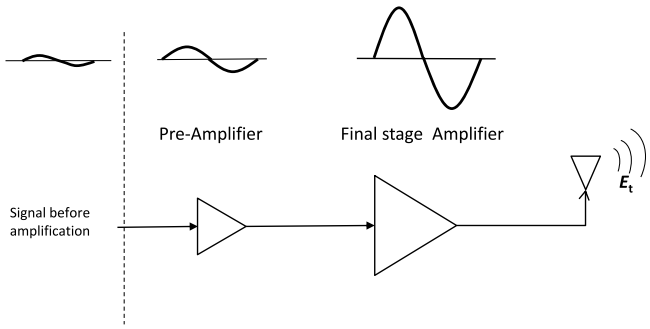

Fig. 3. Typical wireless communications power amplifier chain.

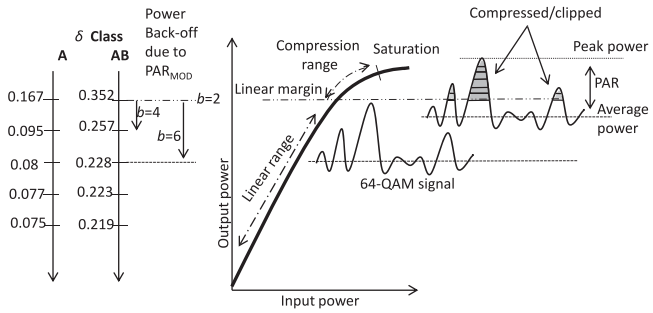

Fig. 4. Linear PA characteristics, efficiency, and power back-off.

Fig. 2 shows that energy efficiency can be achieved at the expense of spectrum efficiency, which matches the famous information theoretic data rate–power consumption cost tradeoff that is shown in [39] and [40] for the AWGN channel. However, the model in Fig. 2, yields a result better suited to the realities of wireless communication systems, because it includes the effect of modulation order (even and odd), fading channel, transmission time, and the link distance between the handset and the base station.

Although E_{t} generally decreases as $\epsilon \to 1$, the transceiver circuits must operate longer, the impact of which is studied in the following sections.

IV. Power Amplifier Dissipated Energy: E_{PAD}

As (7) indicates, the PA dissipated energy is a function of the PA efficiency, δ, which in turn is a function of the amplifier type and the PA back-off due to the amplitude fluctuations of the modulated signal.

A. PA Selection

Fig. 3 shows a wireless communications amplifier chain consisting of a pre-amplifier followed by a final stage. The role of the pre-amplifier—usually[3] class A—is to drive the input signal power to the proper level required for the final stage. In this paper, we use the term "PA" to refer to the final stage because of its dominance in terms of energy consumption and we group the pre-amplifier with the "other" circuits.

PA linearity and efficiency are competing design objectives and both have significant impact on MQAM performance. Because class AB PAs offer an attractive compromise in this design tradeoff they are a popular choice in wireless handsets. Not only do they provide higher maximum drain efficiency, but class AB PAs also have a lower drain efficiency decay rate as the power is being backed off. A typical maximum drain efficiency for a class A PA is $\eta_{\max} = 0.35$ [41], and for a class AB PA $\eta_{\max}$ is in the range 0.5–0.6 [42], [43]. Drain efficiency is defined as the ratio of the output signal power to the DC power consumed in the PA at a given output power [44]. The PA has the maximum drain efficiency $\eta_{\max}$ when it operates with maximum output power (cf., e.g. [41, Fig. 3.11]). However, it is hard to achieve the maximum drain efficiency with a linear modulation such as MQAM because the envelope of the modulated signal changes with the data. Furthermore, the impact of such modulation on different types of PAs is different, as we see next.

[3]For small signals, the power dissipated by the pre-amplifier is negligible.

B. Power Back-Off

The characteristic curve of a PA is shown in Fig. 4, which is based on the Rapp model in [45]. Fig. 4 has regions labeled for linear and non-linear operation. The non-linear region is subdivided into a compression region and a saturation region. For MQAM signals with PAR > 1 (PAR $= 1$ only for BPSK and QPSK because all the points in the I–Q constellation have the same distance from the origin), the signal peak may exceed the limit of linear operation and result in non-linear distortion, the most severe consequence of which is spectral distortion, commonly referred to as "spectral regrowth." There are two main approaches to reduce this distortion [22], [41], [46]–[49]:

1) The first approach is to clip any peak of the signal that exceeds the region of linear operation. This clipping is illustrated in Fig. 4 with the shaded signal areas. Because the MQAM constellation points are represented by amplitude and phase, the clipping approach may result in dramatic loss of information and induce in-band signal distortion [41], [50]. Hence, this approach is not considered herein.
2) The second approach is to use the power back-off procedure, where the average pre-amplifier output level is reduced, which in turn reduces the output level of the final stage. By backing off the same amount as the PAR, the signal peaks remain inside the desired linear range, as shown in Fig. 4. Even though this approach reduces distortion in the modulated signal, the PA efficiency δ decreases proportionally with the PAR/back-off. In this paper, we model the impact of power back-off on the efficiency of different types of linear PA—based on the measured patterns for class A and class B PAs that is given in [41], [51]—as

$$\delta = \frac{\eta_{\max}}{(\text{Power back-off})^{\lambda}} = \frac{\eta_{\max}}{\text{PAR}^{\lambda}}, \tag{16}$$

where λ is the decay rate, which determines the rate of degradation of the PA efficiency with power back-off. The typical values of $\eta_{\max}$ and λ for class A, B, and AB PAs are listed in Table II. Because the value of λ for the class

TABLE II
DRAIN EFFICIENCY CHARACTERISTIC FOR DIFFERENT PA CLASSES

PA type	Decay rate: λ	Typical drain efficiency: $\eta_{\max}$ [39], [40]
Class A	1	0.35
Class AB	(0.5–1)	0.5–0.6
Class B	0.5	0.7

AB case is in between that of class A and class B, a value of 0.6 is considered in this paper. Equation (16) can be stated more clearly for class A PAs as

$$\delta = \frac{0.35}{\text{Power back-off}}, \tag{17}$$

and for class AB PAs as

$$\delta = \frac{0.55}{[\text{Power back-off}]^{0.6}}\ . \tag{18}$$

On the left side of Fig. 4, a numerical scale for (17) and (18) can be seen, which shows a higher maximum drain efficiency and a lower decay rate for class AB PAs compared to class A PAs.[4]

Other techniques, such as pre-distortion, envelope tracking, Doherty PA, etc., are utilized for increasing PA linearity or boosting efficiency, as discussed in the literature [41], [49], [51]–[55]. However, the processing requirements of these techniques are greater than what current handsets can afford and they are mainly used in base stations; therefore, we leave them for future research.

C. PAR

Generally, there are different sources of PAR.[5] In QAM modulation, two types of PAR can be found: PAR of the modulation (PAR_{Mod}), which is a function of b, and PAR of the raised cosine pulse ($\text{PAR}_{\text{roll-off}}$), which is a function α. Therefore, δ can be expressed as a function of b and α as follows:

$$\delta(b,\alpha) = \frac{\eta_{\max}}{\Big(\text{PAR}_{\text{Mod}}(b)\cdot \text{PAR}_{\text{roll-off}}(\alpha)\Big)^{\lambda}}. \tag{19}$$

PAR_{Mod} is defined as

$$\text{PAR}_{\text{Mod}}(b) = \frac{\max_i(|x_i(b)|^2)}{\text{average}_i(|x_i(b)|^2)},\quad b\in\mathbb{N} \tag{20}$$

where x_i is a point in the QAM signal constellation. For even b, this can be expressed as a function of b in closed form as:

$$\text{PAR}_{\text{Mod}}(b) = \frac{3\cdot(\sqrt{2^b}-1)}{\sqrt{2^b}+1},\quad b\in\text{even}(\mathbb{N}). \tag{21}$$

The values of $\text{PAR}_{\text{Mod}}(b)$ for $b=2$ to 12 are listed in Table III. $\text{PAR}_{\text{Mod}}(b)$ for $b=2$ (QPSK) is equal to 0 dB. $\text{PAR}_{\text{Mod}}(b)$ increases with b and converges to a value of 4.5 dB for large modulation orders ($b\geq 10$). This convergence could be welcome news for the PA because the PAR/back-off does not grow arbitrarily large with modulation order.

TABLE III
PAR FOR MQAM [IN DB]

b	2	4	6	8	10	12
$\text{PAR}_{\text{Mod}}(b)$ dB	0	2.5	3.7	4.2	4.5	4.5
$\text{PAR}(b, 0.42)$ dB	3.5	5.7	6.7	6.9	7	7

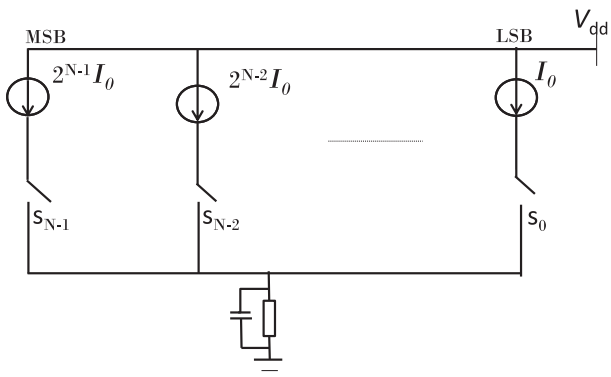

Fig. 5. Binary weighted current steering DAC.

On the other hand, $\text{PAR}_{\text{roll-off}}$ is the PAR that arises from the SRRC pulse shape signal in the transmitter. In the literature, a roll-off factor of $\alpha=1$ is considered as optimum [19]; however, this is true only when the *full* raised cosine pulse is located at the transmitter. In our recent work in [24], we showed that when the SRRC pulse shape is located in the transmitter, a roll-off factor of 0.42 provides the minimum $\text{PAR}_{\text{roll-off}}$. This roll-off factor not only minimizes PAR, but also reduces the bandwidth by 29% relative to $\alpha=1$, according to the bandwidth definition in (4). Thus, $\text{PAR}_{\text{roll-off}}$ with roll-off factor of 0.42 is considered herein. Similar to the case of $\text{PAR}_{\text{Mod}}(b)$ in Table III, the value of $\text{PAR}(b, 0.42)$ converges to 7 dB. These PAR values can be higher if values of α other than the optimum $\alpha=0.42$ are used, as we discussed in our work in [24].

V. OTHER CIRCUIT ENERGY: E_{OTHERS}

We now develop the terms in (8).

A. Digital to Analog Converter (DAC)

The DAC is the first block in the signal chain in the transmitter. The current-steering DAC architecture that is shown in Fig. 5 is consider herein. The power consumption of the DAC has two terms—called static and dynamic [32]—which are

$$P_{\text{DAC}} = \frac{1}{2}V_{\text{dd}}\cdot I_0\cdot\left(2^{N_{\text{DAC}}}-1\right) + N_{\text{DAC}}\cdot C_{\text{p}}\cdot B\cdot V_{\text{dd}}^2\cdot \text{OSR}, \tag{22}$$

where V_{dd} is the power supply voltage, I_0 is the unit current source relating to the least significant bit (LSB), OSR is the oversampling ratio, and C_{p} is the parasitic capacitance of each switch [32]. N_{DAC} is the resolution of the DAC in bits. Based on the signal to noise ratio inside the DAC of approximately

[4] A complexity study for class A, B, and AB PAs is beyond the scope of this paper.

[5] Due to its high PAR, orthogonal frequency division multiplexing (OFDM) is usually not used in a handset/uplink scenario; thus we leave that PAR for future work.

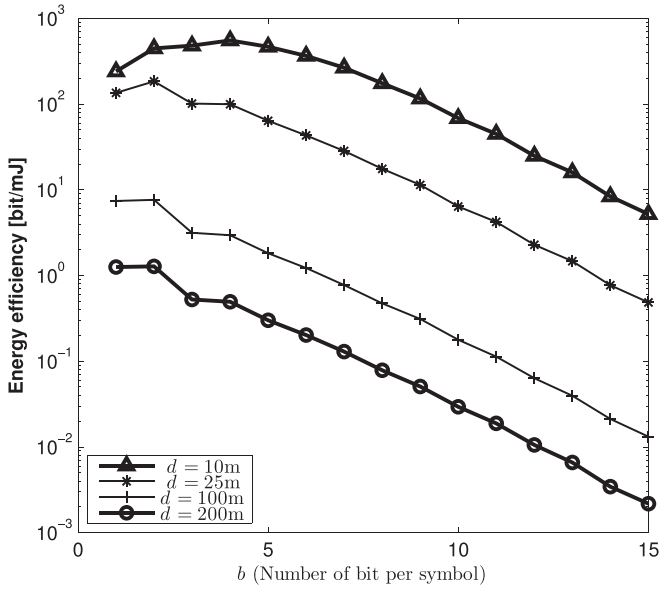

Fig. 6. Energy efficiency vs. b for various values of distance d.

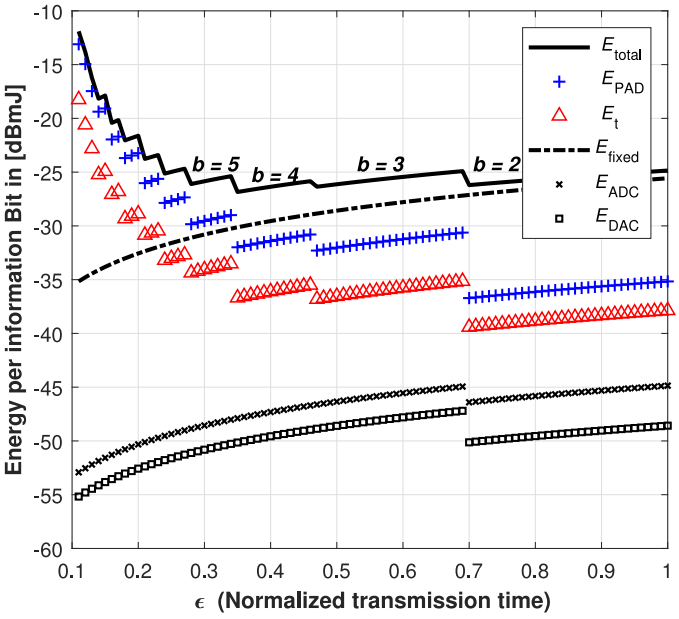

Fig. 7. All energies for $d = 10$ m.

42 dB [32], we derive the following expression of N_{DAC} as a function of PAR_{Mod}

$$N_{\text{DAC}} = \left\lceil 7 + \frac{10\log\{\text{PAR}_{\text{Mod}}(b)\}}{6.02} \right\rceil. \tag{23}$$

Existing models often assume a fixed value of $N_{\text{DAC}} = 8$ or 9 bits, e.g. [16], [19]; however, we allow N_{DAC} to vary in order to more fully capture the energy consumption of the DAC vs. modulation order b. These results can be seen later in Fig. 7, where the assumed values of the DAC parameters are: $V_{\text{dd}} = 3.3$ V, $I_0 = 10$ μA, $C_{\text{p}} = 1$ pF, and OSR $= 4$.

B. Analog to Digital Converter (ADC)

Similar to the DAC, the power consumption of the ADC is expressed as [32]

$$P_{\text{ADC}} = \frac{3V_{\text{dd}}^2 \cdot L_{\min} \cdot B}{10^{-0.152 \cdot N_{\text{ADC}} + 4.838}}, \tag{24}$$

where $L_{\min} = 0.5$ μm is the minimum channel length of the complementary metal oxide semiconductor (CMOS) technology. For simplicity, we assume N_{ADC} is equal to N_{DAC}.[6]

The term $P_{\text{fixed}}T_{\text{on}}$ in (8) models the energy consumption of the remaining circuitry mentioned in Section II-A. The numerical impact of the DAC and ADC on the energy consumption of the wireless handset will be discussed in Section VI-B.

VI. Energy Metrics

A. Energy Efficiency

The energy efficiency U of the wireless handset, in units of bits per joule, can be expressed as a function of b and d using the model we have developed:

$$U(b,d) = \frac{r(b)}{P_{\text{t}}(b,d) + P_{\text{PAD}}(b,d) + P_{\text{DAC}}(b) + P_{\text{ADC}}(b) + P_{\text{fixed}}}, \tag{25}$$

where $r(b) = bR_{\text{s}}$ is the throughput in bits/sec. As discussed earlier, all terms except P_{fixed} change with b and some with both b and d. Eq. (25) can be written as function of b for a given d as

$$U(b) = \frac{bR_{\text{s}}}{P_{\text{t}}(b) + P_{\text{PAD}}(b) + P_{\text{DAC}}(b) + P_{\text{ADC}}(b) + P_{\text{fixed}}}. \tag{26}$$

Because the second derivative[7] of $U(b)$ with respect to b is $U''(b) < 0$ (see Appendices B and C), $U(b)$ is a concave function with respect to b and has an optimum value (global maximum) at b^* for a given distance d.

Fig. 6 shows the concavity of $U(b)$ as a function of b for different values of distance d. The figure shows that increasing communication range decreases the energy efficiency for all b and the location of the optimum b^* on the energy efficiency curve converges to $b = 2$. This is because E_{t} and E_{PAD} dominate the total energy consumption at long communication distances.

Mathematically, the optimum energy efficiency over b can be found by solving the following expression:

$$\underset{b}{\text{maximize}} \quad U(b,d). \tag{27}$$

The solution can be determined by taking the partial derivative with respect to b

$$U(b,d)' = \frac{\partial}{\partial b} \frac{bR_{\text{s}}}{\frac{1}{\delta(b)}P_{\text{t}}(b,d) + P_{\text{DAC}}(b) + P_{\text{ADC}}(b) + P_{\text{fixed}}} = 0, \tag{28}$$

where $\frac{1}{\delta(b)}P_{\text{t}}(b,d) = P_{\text{t}}(b,d) + P_{\text{PAD}}(b,d)$ is the power consumed in the PA. According to (15), $P_{\text{t}}(b) \approx \frac{W}{Z\bar{p}_{eb}} B\sigma^2 N_{\text{F}} G(d)$.

[6]In reality, N_{DAC} and N_{ADC} may have different values, because they face different design requirements, such as spectral regrowth, linearity, etc.

[7]$U(b)$ is continuous and differentiable with respect to b; however, it is evaluated only at integer values.

Hence,

$$\frac{\partial}{\partial b}\frac{bR_{\mathrm{s}}}{\frac{4}{b}\cdot(1-\frac{1}{\sqrt{2^b}})\frac{2^b-1}{3}\frac{1}{\delta(b)}KG(d)+P_{\mathrm{DAC}}(b)+P_{\mathrm{ADC}}(b)+P_{\mathrm{fixed}}}=0, \tag{29}$$

where $K=\frac{1}{\bar{p}_{eb}}B\sigma^2N_{\mathrm{F}}$.

$\delta(b)$ is a function of b via $\mathrm{PAR}_{\mathrm{Mod}}(b)$ by utilizing (19) and (21),

$$\delta(b)=\frac{\eta_{\max}}{\left(\frac{3(\sqrt{2^b}-1)}{\sqrt{2^b}+1}\cdot\mathrm{PAR}_{\text{roll-off}}\right)^{\lambda}}, \tag{30}$$

where $\eta_{\max}$ and λ are listed in Table II for different types of PAs. Now (29) can be stated as

$$\frac{\partial}{\partial b}\frac{bR_{\mathrm{s}}}{(1-\frac{1}{\sqrt{2^b}})\frac{2^b-1}{b}\cdot(\frac{\sqrt{2^b}+1}{\sqrt{2^b}-1})^{\lambda}K_1G(d)+K_2}=0, \tag{31}$$

where $K_1=4/3^{1-\lambda}K\cdot\mathrm{PAR}_{\text{roll-off}}^{\lambda}/\eta_{\max}$, and[8] $K_2\approx P_{\mathrm{fixed}}$. The first derivative of the right hand side of (31) can be found in Appendix B . The final result is

$$\left(\frac{(2^{b^*}-1)(\frac{\sqrt{2^{b^*}}+1}{\sqrt{2^{b^*}}-1})^{\lambda}}{2\sqrt{2^{b^*}}}+2^{b^*}\left(1-\frac{1}{\sqrt{2^{b^*}}}\right)\left(\frac{\sqrt{2^{b^*}}+1}{\sqrt{2^{b^*}}-1}\right)^{\lambda}+\left(\sqrt{2^{b^*}}-2^{b^*}+2\right)\frac{\lambda\cdot(2^{b^*}-1)\sqrt{2^{b^*}}\cdot(\sqrt{2^{b^*}}-1)^{2-\lambda}\log\{2\}}{2\cdot(\sqrt{2^{b^*}}+1)^{3-\lambda}}\right)=\frac{K_2}{G(d)K_1\log\{2\}}. \tag{32}$$

This equation provides the optimum modulation order b^* for energy efficiency at a given d.

The mathematical solution of (32) matches the numerical plot in Fig. 6. For example, at $d=10$ the optimum solution is $b^*=4$, and for large distances b^* decreases to 2. Eq. (32) is considered as a modulation order optimization for energy efficiency at different distances and for different PA types.

In Fig. 6, it is worth noting that the energy efficiency of QPSK ($b=2$) is slightly higher than that of BPSK ($b=1$). The explanation of this is that QPSK has double the throughput and double the transmit power, but with the same fixed value of K_2. Regarding P_{t}, using the appropriate values of W and Z for each modulation in (11), we see that for the same $\bar{p}_{eb}$ the SNR for QPSK is double that of BPSK. And because $\mathrm{PAR}_{\mathrm{Mod}}(1)=\mathrm{PAR}_{\mathrm{Mod}}(2)=1$, we have $\delta(1)=\delta(2)$; therefore, we can write the energy efficiency of BPSK as

$$U(1)=\frac{R_{\mathrm{s}}}{\delta(1)P_{\mathrm{t}}(1)+K_2}, \tag{33}$$

which can be written as

$$U(1)=\frac{2R_{\mathrm{s}}}{2\delta(1)P_{\mathrm{t}}(1)+2K_2}. \tag{34}$$

[8]This assumption can be justified in order to simplify the optimization formula because the values of $P_{\mathrm{DAC}}(b)$ and $P_{\mathrm{ADC}}(b)$ are small relative to the other power terms in the transceiver.

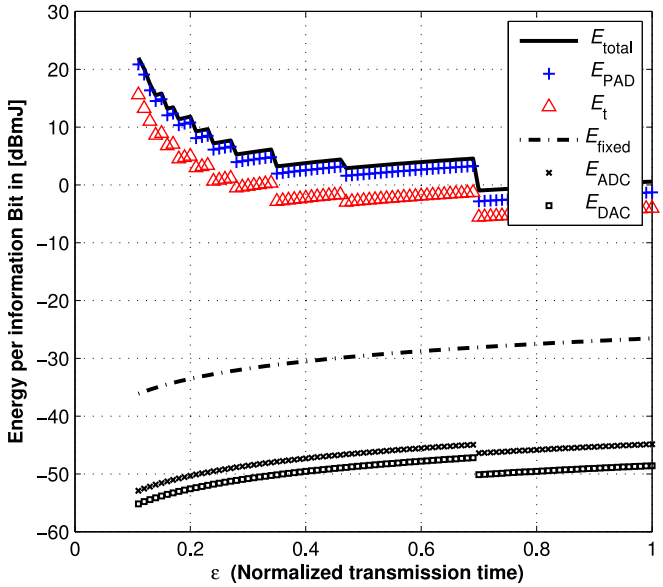

Fig. 8. All energies for $d=200$ m.

However, the energy efficiency of QPSK is

$$U(2)=\frac{2R_{\mathrm{s}}}{\delta(2)P_{\mathrm{t}}(2)+K_2}=\frac{2R_{\mathrm{s}}}{2\delta(1)P_{\mathrm{t}}(1)+K_2}. \tag{35}$$

The denominator of (34) is greater than the denominator of (35) by $K_2\approx P_{\mathrm{fixed}}$, and hence the energy efficiency of BPSK is slightly less than that of QPSK.

B. Energy Consumption

Figs. 7 and 8 show all the energies discussed in our model as a function of normalized transmission time, $\epsilon=T_{\mathrm{on}}/T$, with the appropriate b [see (3)], for short and long distance cases. In both figures, E_{t} and E_{PAD} are generally decreasing with increasing ϵ because the required b is decreasing, as discussed earlier in Fig. 2. E_{fixed} grows proportionally with ϵ. In both figures, we observe the optimum modulation order b, which is optimal in the sense of minimizing the total energy consumption per information bit in the transceiver.

Fig. 7 considers a shorter distance of $d=10$ m, which is applicable in wireless sensor networks, Wi-Fi, or some small cell systems (e.g. femtocell). Fig. 7 shows the required E_{t} and E_{PAD} are relatively small compared to E_{fixed}, which dominates the total energy consumption as ϵ increases and b decreases. This result agrees with the $d=10$ m curve in Fig. 6. In Fig. 7, the minimum total energy occurs at $\epsilon\approx 0.37$. Other papers have observed an optimum energy consumption point similar to this [16], [20]; however, our results in Fig. 7 provide the following additional insights: (a) the optimum modulation order in this particular scenario is identified as $b=4$ (16-QAM), which is associated with $\epsilon\approx 0.37$, (b) energy consumption is separated into many factors, which makes it possible to precisely identify the dominant energy consumer in each scenario.

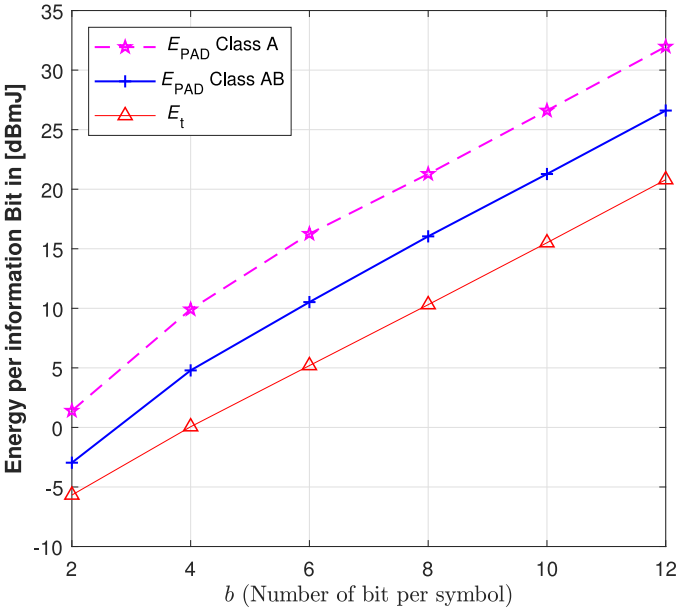

Fig. 9. Total energy for class A and class AB PAs for $d = 200$ m.

Fig. 8 considers a longer distance of $d = 200$ m, and shows that $E_{\rm t}$ and $E_{\rm PAD}$ dominate the total energy consumption for all modulation orders. Here the optimum modulation order for minimizing $E_{\rm total}$ is $b = 2$ (QPSK) at $\epsilon \approx 0.70$. Again, this result agrees with the curves in Fig. 6 for $d > 25$ m. $E_{\rm t}$ in Fig. 8 is exactly that of Fig. 2.

In both figures, because $E_{\rm DAC}$ and $E_{\rm ADC}$ are so small,[9] there are no further insights to be gained by subdividing $E_{\rm others}$ any more; it is better to focus on the PA parameters. These two energies are generally increasing with ϵ. They both shift downward at the point where $b = 2$ occurs, because the required value of $N_{\rm DAC}$ changes from 8 to 7.

C. The Impact of PA Class

Fig. 9 shows that class AB PAs can achieve lower energy consumption than class A PAs, with an advantage of around 4 to 5 dB. This is because class AB PAs have a higher drain efficiency and slower decay with power back-off/PAR, as described in (17) and (18). The values of $\text{PAR}(b, 0.42)$ vs. modulation order are listed in Table III.

The results in Fig. 9 raise a related question, which is: can the linear range of class AB PAs—which is smaller than that of class A PAs—satisfy the required power back-off of higher modulation orders? As Table III shows, $\text{PAR}_{\rm Mod}(b)$ converges to around 4.5 dB for high modulation orders, and thus the amount of PA back-off does not become arbitrarily large. Therefore, class AB PAs can be considered a good design choice for MQAM signals with wireless mobile handsets.

[9]This provides enough justification for our approximation in (31) as $Q \approx P_{\rm fixed}$.

VII. Conclusion

In this paper, we have developed an advanced energy consumption model for wireless cellular systems that takes into account a broad range of parameters. A central idea is to separate PA energy consumption into transmitted energy and dissipated (heat) energy, which allows our model to give design insights that were not possible with previous energy consumption models. Through this separation, our model is able to clearly identify the impact of modulation order on the transmitted energy via the probability of error formula, and on the dissipated energy via the amount of power back-off that occurs to avoid distortion. The results show that class AB PAs can be a good design choice even for high order MQAM modulations, because the PAR converges to 7 dB and that keeps the amount of power back-off from becoming arbitrarily large. We are also able to identify the optimal modulation order in terms of energy-efficiency in different situations, such as transceiver distances, PA classes and efficiencies, and pulse shape. This work provides an important framework for analyzing energy-efficient communications for different wireless systems ranging from cellular networks to wireless internet of things.

Appendix A

As we mention in (9), $\mathbb{E}_h[\cdot]$ is the expected value with respect to the distribution of $|h|^2$, which here is an exponential distribution $f(x) = e^{-x}$ $x \geq 0$. Now, using the definition of $\mathbb{E}_h[\cdot]$, which is

$$\mathbb{E}_h[g(x)] = \int_0^\infty g(x) f(x)\, dx. \tag{36}$$

We can write

$$\bar{P}_{e_b} = W \int_0^\infty Q\left(\sqrt{Z\, x \text{SNR}}\right) f(x)\, dx. \tag{37}$$

Using the definition of the Q function, (37) can be expressed as

$$\bar{P}_{e_b} = W \int_0^\infty e^{-x} \int_{\sqrt{Zx\text{SNR}}}^\infty \frac{1}{\sqrt{2\pi}} e^{-t^2/2} dt dx. \tag{38}$$

For $x = t^2/(Z\text{SNR})$, we obtain

$$\begin{aligned}
\bar{P}_{e_b} &= W \int_0^\infty \int_0^{t^2/(Z\text{SNR})} \frac{1}{\sqrt{2\pi}} e^{-t^2/2} e^{-x} dx dt \\
&= W \frac{1}{\sqrt{2\pi}} \int_0^\infty e^{-t^2/2} \cdot (1 - e^{-t^2/(Z\text{SNR})}) dt \\
&= W \cdot \left(\frac{1}{2} - \frac{1}{\sqrt{2\pi}} \int_0^\infty (e^{-t^2/2 \cdot (1 + 2/(Z \cdot \text{SNR}))}) dt \right) \\
&= \frac{W}{2} \cdot \left(1 - \sqrt{\frac{Z\ \text{SNR}}{2 + Z\text{SNR}}} \right).
\end{aligned} \tag{39}$$

The value $\int_0^\infty \frac{1}{\sqrt{2\pi}} e^{-t^2/2} = Q(0) = 1/2$.

APPENDIX B

$U^{'}(b)$ can be found by taking the first derivative of the right hand side of (31) with respect to b as (40) shown at the bottom of this page.

Then, this can be simplified as (41) shown at the bottom of this page.

APPENDIX C

The second derivative of $U(b)$ with respect to b, $U^{''}(b)$, is obtained by differentiating (41), yielding (42) and (43), both shown at the bottom of this page.

Then, we can write: $U^{''}(b) = -\ G(d)\ K_1 \log\{2\} \cdot \frac{d}{db}\{V \cdot D\}$,

where

$$V = \left(\frac{\sqrt{2^b}+1}{\sqrt{2^b}-1}\right)^{\lambda}, \tag{44}$$

and

$$D = \left(\frac{2^b-1}{2\sqrt{2^b}} + 2^b - \sqrt{2^b} + \frac{\lambda \log\{2\}}{2} \cdot (\sqrt{2^b} - 2^b + 2)\frac{\sqrt{2^b}\cdot(\sqrt{2^b}-1)^3}{(\sqrt{2^b}+1)^2}\right). \tag{45}$$

Hence, the final result can be stated as:

$$U^{''}(b) = -\ G(d)\ K_1 \log\{2\} \cdot \left(V^{'} \cdot D + V \cdot D^{'}\right) < 0, \tag{46}$$

which clearly shows that $U^{''}(b) < 0$ and $U(b)$ is a concave function, where

$$V^{'} = \lambda \cdot \left(\frac{\sqrt{2^b}+1}{\sqrt{2^b}-1}\right)^{\lambda-1} \left(\frac{\sqrt{2^b}\log\{2\}}{2\cdot(\sqrt{2^b}-1)} - \frac{\sqrt{2^b}\cdot(\sqrt{2^b}+1)\log\{2\}}{2\cdot(\sqrt{2^b}+1)^2}\right), \tag{47}$$

and (48) shown at the top of next page.

$$U^{'}(b) = G(d)\ K_1 \cdot \left(\frac{2^b-1}{b}\cdot\left(1-\frac{1}{\sqrt{2^b}}\right)\left(\frac{\sqrt{2^b}+1}{\sqrt{2^b}-1}\right)^{\lambda}\right) + K_2$$
$$-b\,G(d)\ K_1 \cdot \left(\frac{(2^b-1)(1-\frac{1}{\sqrt{2^b}})(\frac{\sqrt{2^b}+1}{\sqrt{2^b}-1})^{\lambda}}{b^2} + \frac{(2^b-1)(\frac{\sqrt{2^b}+1}{\sqrt{2^b}-1})^{\lambda}\log\{2\}}{2b\sqrt{2^b}} + \frac{2^b\cdot(1-\frac{1}{\sqrt{2^b}})(\frac{\sqrt{2^b}+1}{\sqrt{2^b}-1})^{\lambda}\log\{2\}}{b} + \frac{\lambda(2^b-1)(1-\frac{1}{\sqrt{2^b}})\log\{2\}}{b\cdot(\frac{\sqrt{2^b}+1}{\sqrt{2^b}-1})^{1-\lambda}}\left(\frac{2^b\log\{2\}}{2\cdot(\sqrt{2^b}+1)} - \frac{2^b\cdot(2^b-1)\log\{2\}}{2\cdot(\sqrt{2^b}+1)^2}\right)\right). \tag{40}$$

$$= K_2 - \ G(d)\ K_1 \log\{2\} \cdot \left(\frac{(2^b-1)(\frac{\sqrt{2^b}+1}{\sqrt{2^b}-1})^{\lambda}}{2\sqrt{2^b}} + 2^b\cdot\left(1-\frac{1}{\sqrt{2^b}}\right)\left(\frac{\sqrt{2^b}+1}{\sqrt{2^b}-1}\right)^{\lambda} + (\sqrt{2^b}-2^b+2)\frac{\lambda\cdot(2^b-1)\sqrt{2^b}\cdot(\sqrt{2^b}-1)^{2-\lambda}\log\{2\}}{2\cdot(\sqrt{2^b}+1)^{3-\lambda}}\right). \tag{41}$$

$$U^{''}(b) = -\ G(d)\ K_1 \log\{2\} \cdot \frac{d}{db}\left\{\frac{(2^b-1)(\frac{\sqrt{2^b}+1}{\sqrt{2^b}-1})^{\lambda}}{2\sqrt{2^b}} + (2^b-\sqrt{2^b})\left(\frac{\sqrt{2^b}+1}{\sqrt{2^b}-1}\right)^{\lambda} + \frac{\lambda\log\{2\}}{2}\cdot(\sqrt{2^b}-2^b+2)\frac{(2^b-1)\sqrt{2^b}\cdot(\sqrt{2^b}-1)^{2-\lambda}}{(\sqrt{2^b}+1)^{3-\lambda}}\right\}, \tag{42}$$

$$U^{''}(b) = -\ G(d)\ K_1 \log\{2\} \cdot \frac{d}{db}\left\{\left(\left(\frac{\sqrt{2^b}+1}{\sqrt{2^b}-1}\right)^{\lambda}\right)\left(\frac{2^b-1}{2\sqrt{2^b}} + 2^b - \sqrt{2^b} + \frac{\lambda\log\{2\}}{2}\cdot(\sqrt{2^b}-2^b+2)\frac{\sqrt{2^b}\cdot(\sqrt{2^b}-1)^3}{(\sqrt{2^b}+1)^2}\right)\right\}. \tag{43}$$

$$D' = \log\{2\} \cdot \left(\frac{1}{4\sqrt{2^b}} + 2^b - 0.5\sqrt{2^b} + \frac{\lambda \cdot (2^b - 1)^2}{2 \cdot (2^b + 1)^2} \cdot \left(3\, 2^{b-1} \cdot (\sqrt{2^b} - 2^b + 2) \log\{2\} + \sqrt{2^b} \cdot (2^b - 1)(0.5\sqrt{2^b} \log\{2\} - \right.\right.$$

$$\left.\left. 2^b \log\{2\}) + 0.5\sqrt{2^b} \log\{2\} \cdot (\sqrt{2^b} - 2^b + 2) - 2^b \log\{2\} \cdot (\sqrt{2^b} - 2^b + 2) \frac{(2^b - 1)}{(2^b + 1)} \right) \right), \quad (48)$$

REFERENCES

[1] G. Y. Li *et al.*, "Energy-efficient wireless communications: Tutorial, survey, and open issues," *IEEE Wireless Commun.*, vol. 18, no. 6, pp. 28–35, Dec. 2011.

[2] Y. Xu, S. Jiang, and J. Wu, "Toward energy efficient device-to-device content dissemination in cellular networks," *IEEE Access*, vol. 6, pp. 25816–25828, 2018.

[3] F. Han, S. Zhao, L. Zhang, and J. Wu, "Survey of strategies for switching off base stations in heterogeneous networks for greener 5G systems," *IEEE Access*, vol. 4, pp. 4959–4973, 2016.

[4] K. Yang, S. Martin, D. Quadri, J. Wu, and G. Feng, "Energy-efficient downlink resource allocation in heterogeneous OFDMA networks," *IEEE Trans. Veh. Technol.*, vol. 66, no. 6, pp. 5086–5098, Jun. 2017.

[5] J. Wu, S. Rangan, and H. Zhang, *Green Communications: Theoretical Fundamentals, Algorithms, and Applications*. Boca Raton, FL, USA: CRC Press, 2016.

[6] X. Ge, S. Tu, G. Mao, V. Lau, and L. Pan, "Cost efficiency optimization of 5G wireless backhaul networks," *IEEE Trans. Mobile Comput.*, to be published, doi: 10.1109/TMC.2018.2886897.

[7] X. Ge, J. Yang, H. Gharavi, and Y. Sun, "Energy efficiency challenges of 5G small cell networks," *IEEE Commun. Mag.*, vol. 55, no. 5, pp. 184–191, May 2017.

[8] X. Ge, Y. Sun, H. Gharavi, and J. Thompson, "Joint optimization of computation and communication power in multi-user massive MIMO systems," *IEEE Trans. Wireless Commun.*, vol. 17, no. 6, pp. 4051–4063, Jun. 2018.

[9] S. Fu, H. Wen, J. Wu, and B. Wu, "Cross-networks energy efficiency tradeoff: From wired networks to wireless networks," *IEEE Access*, vol. 5, pp. 15–26, 2017.

[10] F. I. Mahmoud and S. A. Mawjoud, "Planning and design of a WCDMA network compatible with existing GSM system in Mosul city," in *Proc. 5th Int. Multi-Conf. Syst., Signals Devices*, 2008, pp. 1–6.

[11] F. E. Mahmood, "Mobile radio propagation prediction for two different districts in Mosul-City," in *MATLAB-A Fundamental Tool for Scientific Computing and Engineering Applications-Volume 2*, London, U.K.: IntechOpen, 2012.

[12] G. Auer *et al.*, "How much energy is needed to run a wireless network?," *IEEE Wireless Commun.*, vol. 18, no. 5, pp. 40–49, Oct. 2011.

[13] F. Tan and S. Fok, "Thermal management of mobile phone using phase change material," in *Proc. 9th Electron. Packag. Technol. Conf.*, 2007, pp. 836–842.

[14] D. Feng, C. Jiang, G. Lim, L. J. Cimini, G. Feng, and G. Y. Li, "A survey of energy-efficient wireless communications," *IEEE Commun. Surv. Tuts.*, vol. 15, no. 1, pp. 167–178, Jan.–Mar. 2013.

[15] A. Gupta and R. K. Jha, "A survey of 5G network: Architecture and emerging technologies," *IEEE Access*, vol. 3, pp. 1206–1232, 2015.

[16] S. Cui, A. J. Goldsmith, and A. Bahai, "Energy-constrained modulation optimization," *IEEE Trans. Wireless Commun.*., vol. 4, no. 5, pp. 2349–2360, Sep. 2005.

[17] S. Cui, A. J. Goldsmith, and A. Bahai, "Modulation optimization under energy constraints," in *Proc. Commun. IEEE Int. Conf.*, 2003, vol. 4, pp. 2805–2811.

[18] Y. Li, B. Bakkaloglu, and C. Chakrabarti, "A comprehensive energy model and energy-quality evaluation of wireless transceiver front-ends," in *Proc. IEEE Workshop Signal Process. Syst. Des. Implement.*, 2005, pp. 262–267.

[19] Y. Li, B. Bakkaloglu, and C. Chakrabarti, "A system level energy model and energy-quality evaluation for integrated transceiver front-ends," *IEEE Trans. Very Large Scale Integration Syst.*, vol. 15, no. 1, pp. 90–103, Jan. 2007.

[20] G. Miao, N. Himayat, and G. Y. Li, "Energy-efficient link adaptation in frequency-selective channels," *IEEE Trans. Commun.*, vol. 58, no. 2, pp. 545–554, Feb. 2010.

[21] C. Schurgers, O. Aberthorne, and M. Srivastava,"Modulation scaling for energy aware communication systems," in *Proc. Int. Symp. Low Power Electron. Des.*, 2001, pp. 96–99.

[22] J. Joung, C. K. Ho, K. Adachi, and S. Sun, "A survey on power-amplifier-centric techniques for spectrum-and energy-efficient wireless communications," *Commun. Surv. Tuts.*, vol. 17, no. 1, pp. 315–333, 2015.

[23] F. Rosas and C. Oberli, "Modulation and SNR optimization for achieving energy-efficient communications over short-range fading channels," *IEEE Trans. Wireless Commun.*, vol. 11, no. 12, pp. 4286–4295, Dec. 2012.

[24] F. Mahmood, E. Perrins, and L. Liu, "Modeling and analysis of power amplifier dissipation energy in wireless handset transceivers," in *Proc. Int. Conf. Comput., Netw. Commun.*, 2018, pp. 1–6.

[25] F. E. Mahmood, E. S. Perrins, and L. Liu, "Modeling and analysis of energy consumption for MIMO systems," in *Proc. Wireless Commun. Netw. Conf.*, 2017, pp. 1–6.

[26] F. E. Mahmood, E. S. Perrins, and L. Liu, "Energy consumption vs. bit rate analysis toward massive MIMO systems," in *Proc. IEEE Int. Smart Cities Conf.*, 2018, pp. 1–7.

[27] Z. Yang, Y. Yuan, and J. He, "Energy aware data gathering based on adaptive modulation scaling in wireless sensor networks," in *Proc. IEEE 60th Veh. Technol. Conf.*, 2004, vol. 4, pp. 2794–2798.

[28] J. Proakis and M. Salehi, *Digital Communications*, 5th ed. New York, NY, USA: McGraw-Hill, 2007.

[29] P. Antognetti, *Power Integrated Circuits Physical Design, and Applications*. New York, NY, USA: McGraw-Hill, 1986.

[30] G. Zhang, S. Khesbak, A. Agarwal, and S. Chin, "Evolution of RFIC handset PAs," *IEEE Microw. Mag.*, vol. 11, no. 1, pp. 60–69, Feb. 2010.

[31] F. Mahmood, E. Perrins, and L. Liu, "Modeling and analysis of energy consumption for RF transceivers in wireless cellular systems," in *Proc. IEEE Global Commun. Conf.*, 2015, pp. 1–6.

[32] M. Gustavsson, J. J. Wikner, and N. Tan, *CMOS Data Converters for Communications*. New York, NY, USA: Springer, 2000.

[33] K. Cho and D. Yoon, "On the general ber expression of one-and two-dimensional amplitude modulations," *IEEE Trans. Commun.*, vol. 50, no. 7, pp. 1074–1080, Jul. 2002.

[34] A. Conti, M. Z. Win, and M. Chiani, "Invertible bounds for M-QAM in Rayleigh fading," *IEEE Trans. Wireless Commun.*, vol. 4, no. 5, pp. 1994–2000, Sep. 2005.

[35] D. Tse and P. Viswanath, *Fundamentals of Wireless Communication*. Cambridge, U.K.: Cambridge Univ. Press, 2005.

[36] A. Goldsmith, *Wireless Communications*. Cambridge, U.K.: Cambridge Univ. Press, 2005.

[37] T. Starr, J. M. Cioffi, and P. J. Silverman, *Understanding Digital Subscriber Line Technology*. Englewood Cliffs, NJ, USA: Prentice-Hall, 1999.

[38] T. S. Rappaport *et al.*, *Wireless Communications: Principles and Practice*, vol. 2. Englewood Cliffs, NJ, USA: Prentice-Hall, 1996.

[39] S. Verdu, "On channel capacity per unit cost," *IEEE Trans. Inf. Theory*, vol. 36, no. 5, pp. 1019–1030, Sep. 1990.

[40] A. Y. Wang and C. G. Sodini, "On the energy efficiency of wireless transceivers," in *Proc. IEEE Int. Conf. Commun.,* 2006, vol. 8, pp. 3783–3788.

[41] S. C. Cripps, *RF Power Amplifiers for Wireless Communications*, 2nd ed. Norwood, MA, USA: Artech House, 2006.

[42] A. Anadigics, Inc., *ALT5020 High Efficiency UMTS E800 LTE Linear*. New Jersey, 2013.

[43] M. Ji, D. Teeter, S. Richard, E. Shull, and D. Mahoney, "Envelope tracking power amplifier design considerations for handset applications," in *Proc. IEEE Topical Conf. Power Amplifiers Wireless Radio Appl.*, Jan. 2016, pp. 27–29.

[44] B. Berglund, J. Johansson, and T. Lejon, "High efficiency power amplifiers," *Ericsson Rev.*, vol. 83, no. 3, pp. 92–96, 2006.

[45] F. Raab, "Efficiency of outphasing RF power-amplifier systems," *IEEE Trans. Commun.*, vol. 33, no. 10, pp. 1094–1099, Oct. 1985.

[46] P. B. Kenington, *High Linearity RF Amplifier Design*. Norwood, MA, USA: Artech House, Inc., 2000.

[47] S. W. Amos and M. James, *Principles of Transistor Circuits*. London, U.K.: Butterworths, 1984.

[48] S. L. Miller and R. J. O'Dea, "Peak power and bandwidth efficient linear modulation," *IEEE Trans. Commun.*, vol. 46, no. 12, pp. 1639–1648, Dec. 1998.
[49] X. Zhang, L. E. Larson, and P. Asbeck, *Design of Linear RF Outphasing Power Amplifiers*. Norwood, MA, USA: Artech House, 2003.
[50] H. Ochiai, "An analysis of band-limited communication systems from amplifier efficiency and distortion perspective," *IEEE Trans. Commun.*, vol. 61, no. 4, pp. 1460–1472, Apr. 2013.
[51] F. H. Raab *et al.*, "Power amplifiers and transmitters for RF and microwave," *IEEE Trans. Microw. Theory Techn.*, vol. 50, no. 3, pp. 814–826, Mar. 2002.
[52] J. Jeong, D. F. Kimball, M. Kwak, P. Draxler, and P. M. Asbeck, "Envelope tracking power amplifiers with reduced peak-to-average power ratio RF input signals," in *Proc. Radio Wireless Symp.*, 2010, pp. 112–115.
[53] P. Colantonio, F. Giannini, R. Giofrè, and L. Piazzon, "The AB-C Doherty power amplifier. Part I: Theory," *Int. J. RF Microw. Comput.-Aided Eng.*, vol. 19, no. 3, pp. 293–306, 2009.
[54] J. C. Pedro, N. B. Carvalho, C. Fager, and J. A. Garcia, "Linearity versus efficiency in mobile handset power amplifiers: A battle without a loser," *Microw. Eng. Eur.*, 2004.
[55] S. P. Stapleton and A. E. EDA, "Digital predistortion of power amplifiers," Agilent Technol. Inc., Santa Clara, CA, USA, 2005.

Farhad Mahmood (S'13–M'19) received the B.S. and M.S. degrees from University of Mosul, Mosul, Iraq, in 2005, and 2008, respectively, and the Ph.D. degree from The University of Kansas, Lawrence, KS, USA, in 2019, all in electrical engineering. He is currently a Lecturer in the Electrical Engineering Department, College of Engineering, University of Mosul. From 2012 to 2019, he was with Higher Committee of Education Development in Iraq Scholar to obtain his Ph.D., where he received the Telemetry Award in 2019. Prior to his Ph.D. study, he was with the Communication and Electronic Lab, University of Mosul.

Dr. Mahmood is a member of the IEEE Young Professionals Society since 2013. His research interests include wireless communication, energy efficiency, radio network planning, position location, and antennas design.

Erik Perrins (S'96–M'05–SM'06) received the B.S. (*magna cum laude*), M.S., and Ph.D. degrees from Brigham Young University, Provo, UT, USA, in 1997, 1998, and 2005, respectively, all in electrical engineering. From 1998 to 2004, he was with Motorola, Inc. Schaumburg, IL, USA, where he was engaged in research on land mobile radio products. Since August 2005, he has been with the Department of Electrical Engineering and Computer Science, University of Kansas, Lawrence, where he is currently the Charles E. & Mary Jane Spahr Professor and Department Chair. Since 2004, he has been an Industry Consultant on problems such as reduced-complexity receiver design, receiver synchronization, and error control coding. His current research interests include digital communication theory, synchronization, channel coding, energy efficient communications, and complexity reduction in receivers.

Dr. Perrins is a member of the IEEE Aerospace and Electronic Systems Society and the IEEE Communications Society. He was an Editor and an Area Editor for the IEEE TRANSACTIONS ON COMMUNICATIONS from 2007–2018, and was the Chair of the Communication Theory Technical Committee within the IEEE Communications Society from 2017–2018.

Lingjia Liu (SM'15) received the B.S. degree in electronic engineering from Shanghai Jiao Tong University, Shanghai, China, and the Ph.D. degree in electrical and computer engineering from Texas A&M University, Uvalde, TX, USA. He is currently an Associate Professor in the Bradley Department of Electrical and Computer Engineering, Virginia Tech. He is also an Associate Director for affiliate relations in Wireless@Virginia Tech. Prior to joining Virginia Tech, he was an Associate Professor in the EECS Department, University of Kansas. He was with the Standards and Mobility Innovation Lab, Samsung Research America (SRA) where he received Global Samsung Best Paper Award in 2008 and 2010, respectively. At SRA, he was leading Samsungs efforts on multiuser MIMO, CoMP, and HetNets in 3GPP LTE/LTE-Advanced standards. His general research interests mainly lie in emerging technologies for 5G cellular networks and beyond including machine learning for wireless networks, massive MIMO, massive machine type communications (MTC), Internet of Everything (IoE), and mmWave communications. He received Air Force Summer Faculty Fellow from 2013 to 2017, Miller Scholar at KU in 2014, Miller Professional Development Award for Distinguished Research at KU in 2015, 2016 IEEE GLOBECOM Best Paper Award, 2018 IEEE ISQED Best Paper Award, 2018 IEEE TCGCC Best Conference Paper Award, and 2018 IEEE TAOS Best Paper Award. He is currently an Editor for the IEEE TRANSACTIONS ON WIRELESS COMMUNICATIONS, and an Associate Editor for the IEEE TRANSACTIONS ON NEURAL NETWORKS AND LEARNING SYSTEMS.